ELSEVIER

Sensors and Actuators 81 (2000) 359–362

SENSORS AND ACTUATORS A PHYSICAL

www.elsevier.nl/locate/sna

Switching behavior of small soft magnetic elements

K. Ramstöck [a,*], J.J.M. Ruigrok [b], J.C. Lodder [a]

[a] *MESA Research Institute, ISTG, University Twente, 7500 AE Enschede, Netherlands*
[b] *Philips Research Laboratories Eindhoven, Prof. Holstlaan 4, 5656 AA Eindhoven, Netherlands*

Abstract

Hysteretic properties of submicron-sized soft magnetic elements as they might be used in integrated field sensors are computed. A new 3D micromagnetic simulation program was used which requires only workstation computing power. Results are scrutinized using previously established techniques. The influence of object shape and size is investigated and related to experimental findings reported in the literature.

Keywords: Switching behavior; Small soft magnetic elements; Hysteretic properties; 3D micromagnetic simulation

1. Introduction

Small soft magnetic elements are frequently investigated using micromagnetic modelling. The model reported here is fully 3D; the magnetization m can point in any direction and may be a function of all three spatial variables $r=(r_x,\ r_y,\ r_z)$. It considers exchange coupling energy E_{ex}, uniaxial anisotropy energy E_k, stray field energy E_d and external field energy E_z:

$$E_{total}(m(r)) = E_{ex} + E_k + E_d + E_z. \quad (1)$$

For each program run, a minimum of this energy with respect to m is obtained using suitable minimization techniques. Starting the optimization with various initial configurations, different stable configurations are found. Their behavior as function of applied field is investigated, thus allowing to construct hysteresis loops. The model thus excludes dynamic effects which play a role only in very high frequency ($\sim$ GHz) applications and thermal effects which play no role for this combination of material parameters and temperature.

2. Numerical procedure

2.1. Computational techniques

The program used is a straightforward extension of the one described in Ref. [1] to three dimensions. The minimization procedure has been improved to reduce computation time. Due to the constraints imposed by the FFT method used for stray field computation, a uniform grid and cuboid computational volume are always necessary. The computational volume is thus divided into Z equal cuboid cells, with the interpolated magnetization inside each cell defined by the values in the cell edges. The edge lengths of each cell Δ_x, Δ_y and Δ_z should be roughly the same. Arbitrary sample shapes are handled by using a computational volume which contains the shape completely. At the voids such included the magnetization is simply set to zero. To improve the convergence of this

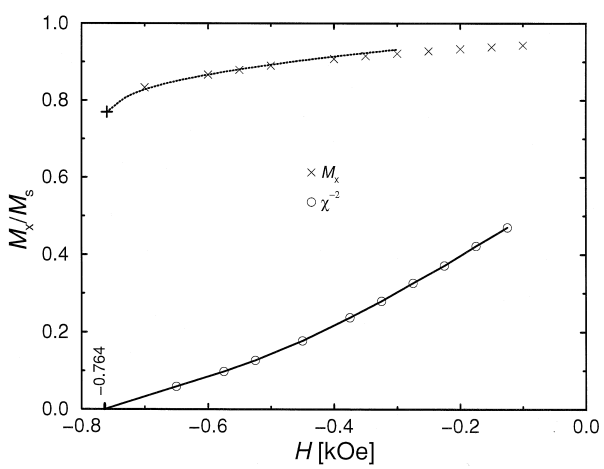

Fig. 1. The susceptibility $\chi = \mathrm{d}M_x/\mathrm{d}H$ was found to diverge at the critical field. The $1/\chi^2$ was extrapolated towards zero to find the critical field.

* Corresponding author.

0924-4247/00/$ - see front matter
PII: S0924-4247(99)00111-9

somewhat crude approach, for each cell the volume fraction filled with sample material is stored. This is considered as exchange, anisotropy and external field energy density are integrated over the computational volume. The stray field energy, which is non-local and thus has no local density, is not affected by this approach. Surface charges are avoided by using one additional layer of volume charges outside the sample. The error such introduced is well-behaved in the sense that it vanishes as the discretization is refined.

2.2. Evaluation of simulation results

Once the problem is stated in mathematical terms, it has a well-defined solution, which is independent of the actual computational techniques used. This is hard to achieve in

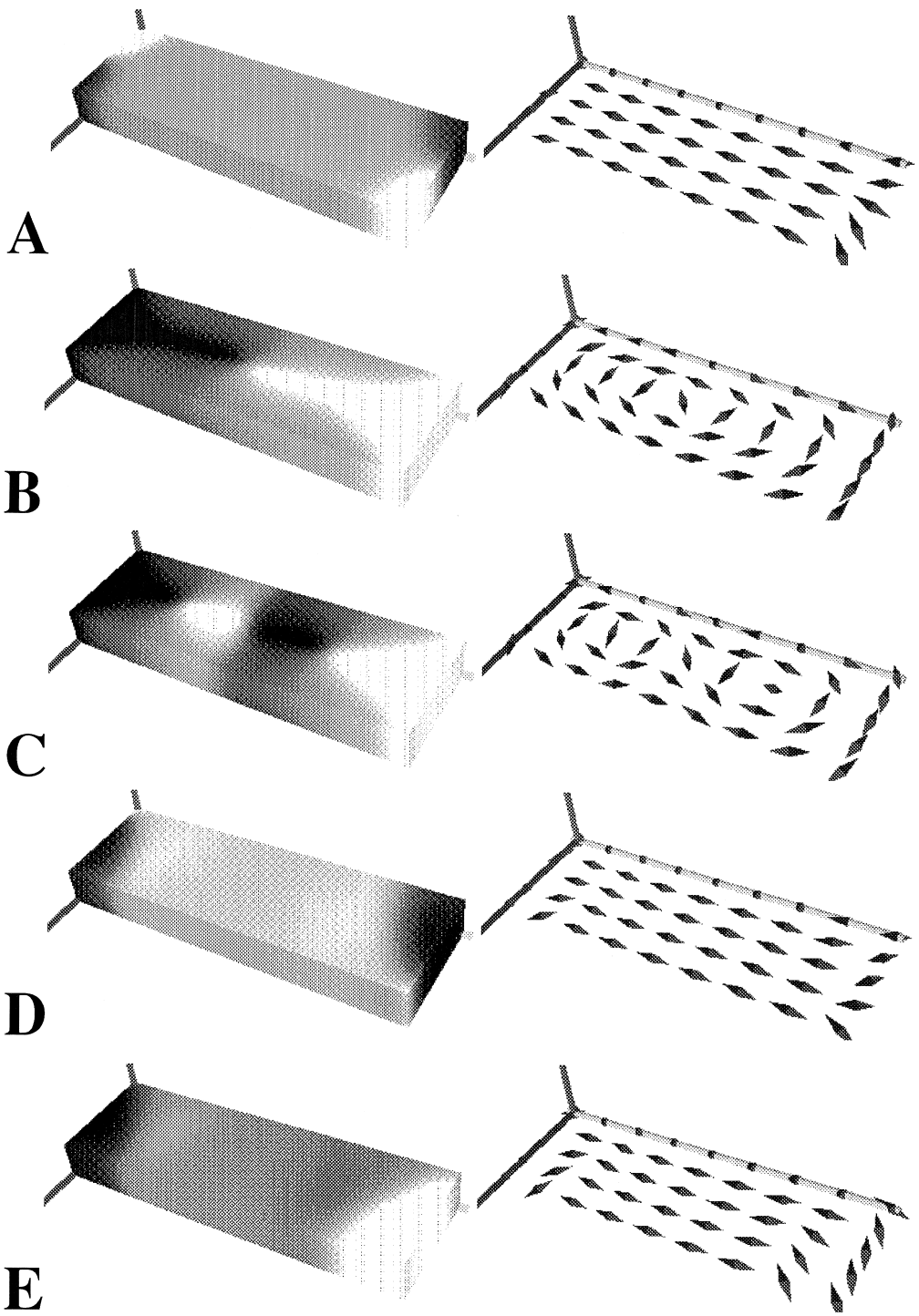

Fig. 2. The five stable states in the 270×90 nm particle at zero field. Shown are the transverse components of m as grayscale and vector plots. (A) Saturated state; (B, C) demagnetized states; (D, E) remanent states. All states are shown at zero applied field, where (A) is almost unstable.

Table 1
Energies at zero field and critical fields of the different states for different aspect ratio

Size (nm)			AR	State B		State D	
D	L	W		E/K_d	$H_{c,1}$ (kOe)	E/K_d	$H_{c,2}$ (kOe)
30	180	90	2:1	0.085	0.53	0.110	−0.61
30	270	90	3:1	0.098	0.35	0.078	−0.78
30	540	90	6:1	0.105	–	0.041	−0.85
60	540	180	3:1	0.037	0.25	–	–

The field is applied in easy axis direction. Energies are measured in units of K_d, which is 420 kJ/m^3 for permalloy. The results given are for $\Delta = 0.62\,\delta_{ex}$. Results for $\Delta = 0.81\,\delta_{ex}$ differ up to 5%.
AR: Aspect ratio L/W (length/width). Film thickness is denoted by D.

practice, as a recent benchmark revealed [2]. The following three sources of errors have been considered in this analysis: insufficient relaxation, insufficient discretization and false switching. Further, states can be found which are mathematically stable but not physically. This was investigated by applying small off-axis fields.

2.2.1. Insufficient relaxation

Insufficient relaxation occurs if the termination criterion used in the iteration cycle is not strict enough. Here, the maximum torque acting on any local magnetization was monitored. The iteration was stopped if this value dropped below a certain threshold [1]. As a check for the threshold value, progress was monitored each time the maximum torque was reduced by a factor three. For all variables checked, a stable state was reached after sufficient iteration steps.

2.2.2. Insufficient discretization

Errors introduced by the discretization cannot be avoided. To investigate their influence on the results, at least two different discretizations which satisfy Eq. (2) are always used.

$$\Delta < \delta_{ex} \tag{2}$$

where: $\Delta := \max(\Delta_x, \Delta_y, \Delta_z)$; δ_{ex} is sqrt(A/K_d); A is the exchange stiffness constant; K_d is the stray field energy constant $2\pi M_s^2$ (CGS); Δ_x, Δ_y and Δ_z are the discretization cell sizes.

The difference in the energy can then be used as a quality measure. For all examples investigated in detail, $Z^{-1/3}$ behavior was found always as Eq. (2) was satisfied.

Computational resources of the computer used limit the total number of discretization cells Z to about 250,000. Together with the constraint (2), this limits the magnetic volume that can be modelled.

2.2.3. False switching

The algorithm sometimes finds the reversed state, although the state with the average magnetization M aligned against the external field is still stable. This problem is addressed by extrapolating the square of the inverse susceptibility towards zero [3]. Close to the critical field H_c, this quantity vanishes as the susceptibility diverges (Fig. 1).

3. Results

The following computations were all done for elongated thin film elements of aspect ratio 2:1, 3:1 and 6:1. Easy axis was chosen in long $(=x)$ direction. The reduced anisotropy $Q = K_u/K_d$ was set to 2.5×10^{-4}. The saturation magnetization M_s was set to 1 kG and the exchange length to 5 nm. Element sizes were 180, 270 and 540×90 nm at 30 nm film thickness and 540×180 nm at 60 nm film thickness.

3.1. Cuboid film elements

The following five states were found (Fig. 2). The states relevant for the hysteretic behavior were identified as the demagnetized state B and the remanent states D and E, which behaved almost exactly the same. For the aspect ratio 3:1, the saturated state A was found to be very unstable at zero field. A field of 0.1% H_c perpendicular to the easy axis triggered switching. Due to inevitable misalignment this state A will thus not contribute in real samples, and reversal always be observed via the D state. The flux-closure structures B and C behaved mostly the same, with B showing the lower energy. Only B was thus investigated in more detail (see Table 1). Due to symmetry, B switches at the critical field $\pm H_{c,1}$. The remanent state D was found to be stable also in a field antiparallel to m, $H_{c,2}$ is thus always negative (Fig. 3).

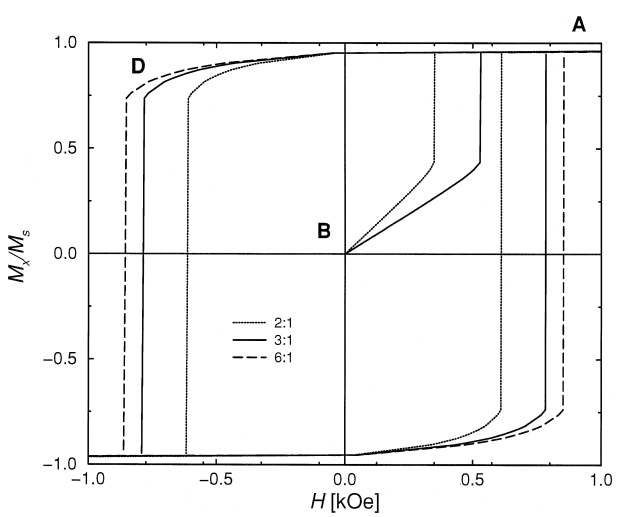

Fig. 3. Hysteresis loop of permalloy particles made of 30 nm film for different aspect ratios. Due to the small shape, the soft permalloy shows a square curve and high remanence.

Table 2
Critical fields for trapeze cross section of the elements

Inclined edge	Inclination angle (in degrees)	Critical field $H_{c,2}$ (kOe)
Short	75	−0.78
Long	75	−0.80
Long	45	−0.87

Whereas inclining the short sides has little influence on the critical field, an inclination of the long sides increases $H_{c,2}$ as the magnetization gets trapped in the corners. $H_{c,2}$ is −0.78 kOe for 90° edge angle (Table 1).

From these results, the hysteresis loops in Fig. 3 are constructed. The 60-nm element is not included as not enough states were investigated yet. Computing time for one field step is ca. 30 min for $270 \times 90 \times 30$ nm and 5 h for $540 \times 180 \times 60$ nm.

3.2. Shape influence

The precise shape of the element edge is known to have a significant influence on the magnetic behavior [4]. It is thus an important degree of freedom for engineering. The following critical fields were found for $270 \times 90 \times 30$ nm elements with edge angles other than 90° on either the long or the short sides (see Table 2).

4. Discussion

No observations on elements in the size investigated here are reported in literature. However, the remanent state D looks very similar to what is observed on larger elements [5]. Ref. [6] contains a systematic analysis of aspect ratio influence. Three different types of hysteresis loops are reported as film thickness and aspect ratio are modified. Whereas the states found there are more complex due to the larger size, the principal behavior is reproduced: above a certain aspect ratio, the high-remanence state will become energetically more favorable than the demagnetized state. This is due to the increase in wall energy for the demagnetized state, where more wall surface is needed as the aspect ratio is increased. On the other hand, the total energy of the remanent state stays roughly the same. Film thickness influences wall type [7] and thus the aspect ratio where this happens. The values for the critical fields found in [6] are much smaller (~10–50 Oe, depending on element investigated) than the numerical values obtained here. This is attributed to the smaller size of the elements investigated and defects in the samples which aid reversal. Note in this respect the decrease in $H_{c,1}$ for the 60-nm film element.

5. Conclusions

Small soft magnetic elements were successfully modelled using only workstation computing power. Realistic states were found and reasonable size dependencies found. Shape influence needs further investigation.

Acknowledgements

This work has been funded by the Dutch FOM. We are grateful for discussions with R. Coehoorn and J. Chapman.

References

[1] D.V. Berkov, K. Ramstöck, A. Hubert, Solving micromagnetic problems, Phys. Status Solidi A 137 (1993) 207–225.
[2] http://www.ctcms.nist.gov/~rdm/mumag.org.html.
[3] W. Rave, K. Ramstöck, A. Hubert, Corners and nucleation in micromagnetics, J. Magn. Magn. Mat. 183 (1998) 329–333.
[4] R. Mattheis, K. Ramstöck, J. McCord, Formation and annihilation of edge walls in thin-film permalloy strips, IEEE Trans. Magn. 33 (5) (1997) 3993–3995.
[5] J.N. Chapman, P.R. Aitchison, K.J. Kirk, S. McVitie, J.C.S. Kools, M.F. Gillies, Direct observation of magnetization reversal processes in micron-sized elements of spin-valve material, J. Appl. Phys., in press.
[6] S.J. Hefferman, J.N. Chapman, S. McVitie, In-situ magnetizing experiments on small regularly shaped permalloy particles, J. Magn. Magn. Mat. 95 (1991) 76–84.
[7] K. Ramstöck, W. Hartung, A. Hubert, The phase diagram of domain walls in narrow magnetic strips, Phys. Status Solidi A 155 (1996) 505–518.